TWO-DIMENSIONAL MAGNETIC ALGORITHM TO DETECT REINFORCING STEEL

By Craig M. Newtson,[1] Student Member, ASCE, and Marc O. Eberhard,[2] Associate Member, ASCE

ABSTRACT: A two-dimensional algorithm has been developed to determine the locations and sizes of steel bars in reinforced concrete members. This algorithm uses magnetostatic relationships to relate measured distortions in the magnetic field outside of a concrete member to the distribution of steel within the member. An optimal solution for the locations and sizes of the steel bars is determined by minimizing the difference between measured and computed distortions of the magnetic field. Finite-element analyses were conducted to simulate the interaction between steel bars and an imposed magnetic field. On the basis of the simulated magnetic distortion, the algorithm accurately identified the location and size of a single bar even when 20% error was induced in the magnetic distortions. The algorithm also identified two bars spaced horizontally or vertically. However, if one bar was much closer to the receivers than the other, only the closest bar was identified accurately. When 10% error was induced in the simulated magnetic distortions, the algorithm accurately located two bars only when the areas were already known.

INTRODUCTION

In many reinforced concrete structures, it is necessary to nondestructively determine the locations and sizes of the reinforcing bars. This information is often desired to assess the safety of aging structures and inspect new construction. Currently, the geometry of the reinforcement is most often determined with induction meters, which rely on the magnetic properties of the steel. Induction meters provide acceptable results when the reinforcement configuration is simple. However, nondestructive evaluation with induction meters is less reliable when the geometry of the reinforcement is complicated by the presence of closely spaced bars, stirrups, and ties (Lauer 1991).

The ability to evaluate civil engineering structures would significantly improve if a magnetic method were available to decipher complex reinforcement configurations. As a step toward this goal, this paper presents the basis of a two-dimensional, magnetostatic technique to determine the locations and sizes of reinforcing bars. To implement this technique, a magnetic field ($\mathbf{B}_0$) is applied to a reinforced concrete member, and the distortion of the field ($\mathbf{B}''$), caused by the steel within the member, is measured in several locations. A possible configuration is shown schematically in Fig. 1. The algorithm computes the reinforcement configuration whose corresponding magnetic distortion most resembles the measured distortions.

After presenting an overview of the reconstruction algorithm, the two-dimensional relationships that support the algorithm are derived. The algorithm was applied to one-bar and two-bar configurations for which input data were provided by finite-element simulations. To investigate the reconstruction algorithm's sensitivity to measurement errors, simulations of selected geometries were repeated with various amounts of error.

[1]Grad. Res. Asst., Dept. of Civ. Engrg., Univ. of Washington, FX-10, Seattle, WA 98195.

[2]Asst. Prof., Dept. of Civ. Engrg., Univ. of Washington, Seattle, WA.

Note. Discussion open until January 1, 1996. To extend the closing date one month, a written request must be filed with the ASCE Manager of Journals. The manuscript for this paper was submitted for review and possible publication on August 2, 1994. This paper is part of the ***Journal of Materials in Civil Engineering***, Vol. 7, No. 3, August, 1995. ©ASCE, ISSN 0899-1561/95/0003-0141–0147/$2.00 + $.25 per page. Paper No. 8977.

OVERVIEW OF ALGORITHM

A two-dimensional algorithm is proposed to determine locations and sizes of steel reinforcing bars in concrete. The underlying physical phenomenon is the same as that exploited by the three-dimensional algorithm presented by Pla et al. (1994). The two-dimensional reconstruction procedure consists of the following steps:

1. A long coil, generating a magnetic field $\mathbf{B}_0$, is used to magnetize the steel within a concrete member. This magnetization induces an additional field, $\mathbf{B}''$, at all points in space (Fig. 1).
2. The two vector components of the total magnetic field $\mathbf{B}$ normal to the length of the bars are measured outside the member. This field is the sum of $\mathbf{B}_0$ and $\mathbf{B}''$.
3. The measured distortion in the magnetic field $\mathbf{B}''_{meas}$, caused by the steel inside the member, is determined by subtracting the magnetic field generated by the coil from the total magnetic field (i.e., $\mathbf{B}''_{meas} = \mathbf{B} - \mathbf{B}_0$).
4. For a trial configuration of reinforcing bars (trial x-coordinates, y-coordinates, and area values for an assumed number of bars), $\mathbf{B}_0$ at the center of each bar is computed.
5. The magnetic dipole density $\mathbf{M}$ for each trial bar is determined by simultaneously solving two sets of equations. The first equation relates $\mathbf{M}$ to the magnetic field to which the bar is subjected. This field is the sum of the imposed magnetic field $\mathbf{B}_0$ and the magnetic field caused by magnetization of the other bars $\mathbf{B}''$.

$$\mathbf{M} = \frac{\chi_m}{\mu_0(1 + 0.5\chi_m)}(\mathbf{B}_0 + \mathbf{B}'') \tag{1}$$

where χ_m = the magnetic susceptibility of the steel; and μ_0 = the permeability constant in vacuum ($4\pi 10^{-7} N/$

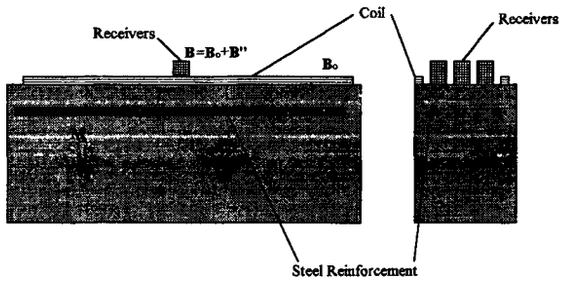

FIG. 1. Magnetic Imaging Technique

A^2). The second equation relates magnetic distortion at the location of one bar $\mathbf{B}''$ to the magnetic dipole density $\mathbf{M}$ at another:

$$\begin{pmatrix} B_x'' \\ B_y'' \end{pmatrix} = \frac{\mu_0 A_{steel}}{2\pi(x^2 + y^2)^2} \begin{bmatrix} x^2 - y^2 & 2xy \\ 2xy & y^2 - x^2 \end{bmatrix} \begin{pmatrix} M_x \\ M_y \end{pmatrix} \quad (2)$$

where x and y are the distances along the x- and y-axes, respectively, from the bar having the influence to the bar being investigated. Both (1) and (2) are derived in the next section.

6. Eq. (2) is used to calculate the distortion in the magnetic field at the receivers, $\mathbf{B}''_{calc}$. In this step, $\mathbf{M}$ is the magnetic dipole density at a bar, and x and y are the distances from the bar to the receiver.
7. The sum of squared differences (SSD) is computed for all of the receivers:

$$SSD = (\mathbf{B}''_{meas} - \mathbf{B}''_{calc})^T(\mathbf{B}''_{meas} - \mathbf{B}''_{calc}) \quad (3)$$

8. New configurations are selected, and steps 4–7 are repeated until SSD is minimized. This minimization results in the identification of the locations and sizes of reinforcing bars that would cause magnetic distortions most similar to those measured.

TWO-DIMENSIONAL RELATIONSHIPS

The proposed algorithm relies heavily on (1) and (2), which are derived in this section. In deriving these equations, the steel is assumed to be square in cross section and infinitely long. It is also assumed that the magnetic field is constant along the length of the bar and over the bar's cross section.

Magnetization Induced by Ambient Magnetic Field

A relationship between magnetic dipole density ($\mathbf{M}$) and ambient magnetic field ($\mathbf{B}_0 + \mathbf{B}''$) can be developed for the geometry shown in Fig. 2. The reinforcing bar is square in cross section (xy-plane), and extends to infinity in the z-direction. If $\mathbf{M}$ is assumed constant within the reinforcing bar, the magnetization can be modeled with a current distribution on the surface of the steel (Nayfeh and Brussel 1985). For this geometry, the current distribution consists of differential current loops. The magnitudes of the currents are $M_x dx$ and $M_y dy$ for loops about the x-axis and y-axis, respectively (Fig. 2).

Magnetization of the steel causes a magnetic field $\mathbf{B}'$ within the bar. This field can be determined from the current distribution. If the bar extends to infinity, only currents along the length (z-direction) of the bar contribute to $\mathbf{B}'$. Therefore, the x- and y-components of the magnetic field caused by a single loop can be computed as the sum of the contributions from two, infinitely-long, wires. Starting with Biot-Savart's law (Nayfeh and Brussel 1985), it can be shown that the magnetic field generated by a single wire with current I is:

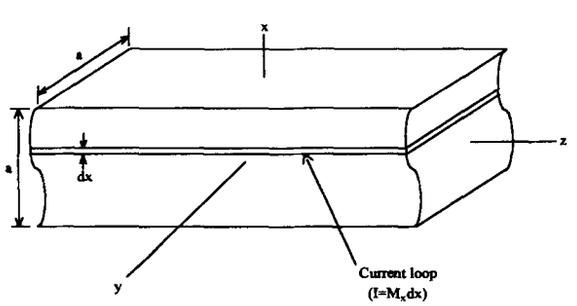

FIG. 2. Differential Current Loop on Surface of Rectangular Bar

$$\mathbf{B} = \frac{\mu_0 I}{2\pi r}\left(\mathbf{k} \times \frac{\mathbf{r}}{r}\right) \quad (4)$$

where $\mathbf{r}$ = the two-dimensional vector from the wire centroid to the point being considered (the center of the bar); r = the magnitude of vector $\mathbf{r}$; and $\mathbf{k}$ = a unit vector parallel to the direction of current.

The resulting magnetic field $\mathbf{B}'$ is the sum of the contributions of all the differential current loops. For the x-component, the following is obtained:

$$B_x' = \int_{-a/2}^{a/2} \frac{\mu_0 M_x}{\pi\sqrt{\left(\frac{a}{2}\right)^2 + x^2}}\, dx \quad (5)$$

Performing this integration for both the x- and y- components results in:

$$\mathbf{B}' = \frac{\mu_0}{2}\mathbf{M} \quad (6)$$

For low values of magnetic intensity, magnetization varies linearly with the magnetic field (Bleaney and Bleaney 1965):

$$\mathbf{M} = \frac{\chi_m(\mathbf{B}_0 + \mathbf{B}'' + \mathbf{B}')}{\mu_0(1 + \chi_m)} \quad (7)$$

Substituting (6) into (7) allows the magnetic dipole density to be expressed as a function of the ambient magnetic field at a reinforcing bar. This relationship was previously defined as (1).

Two-Dimensional Magnetic Dipole Formula

The two-dimensional magnetic dipole formula in (2) relates distortion in the magnetic field, $\mathbf{B}''$, at one point to the magnetic dipole moment at another point. This relationship may be derived from the three-dimensional magnetic dipole formula (Nayfeh and Brussel 1985):

$$\mathbf{B}'' = \frac{\mu_0}{4\pi R^3}\left[3\left(\mathbf{m}\cdot\frac{\mathbf{R}}{R}\right)\frac{\mathbf{R}}{R} - \mathbf{m}\right] \quad (8)$$

where $\mathbf{R}$ = the vector from the magnetized material to the point where the magnetic field is being investigated; and $\mathbf{m}$ = the magnetic dipole moment.

In the two-dimensional case, the reinforcing bars are assumed to be infinitely long and uniformly magnetized by a long coil. Therefore, the distortion in the magnetic field at a point is the sum of the distortions caused by an infinite number of differential volumes, as shown in Fig. 3.

The x-component of $\mathbf{B}''$ caused by a single differential element, dB_x'', can be obtained by expanding (8) and substituting $\mathbf{M}A_{steel}dz$ for $\mathbf{m}$:

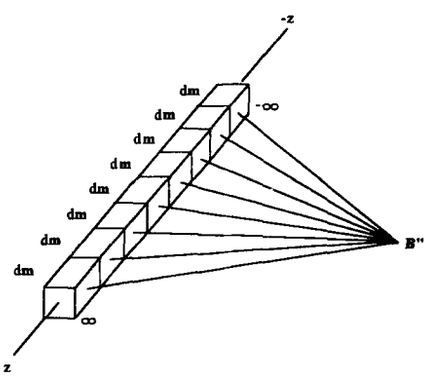

FIG. 3. Differential Magnetic Dipole Moments Causing Distortion in Magnetic Field

$$dB''_x = \frac{\mu_0 A_{steel}\, dz}{4\pi(x^2 + y^2 + z^2)^{5/2}} [3(M_x x + M_y y + M_z z)x - M_x(x^2 + y^2 + z^2)] \quad (9)$$

where the dimensions x, y, and z are measured from the center of the magnetized element to the point at which the distortion in the magnetic field is being evaluated. Similar expressions may be obtained for dB''_y and dB''_z. Integrating these expressions from negative infinity to positive infinity in the z-direction leads to (2). There is no need to measure the z-component of the magnetic field because, theoretically, B''_z is zero.

IMPLEMENTATION OF ALGORITHM

The reconstruction algorithm (steps 4–8) has been implemented with the software package MATLAB (Sigmon 1992). The user provides initial trial values of the bar coordinates and areas. Then, the program computes the distortion in the magnetic field at the receivers as well as the difference between the computed and measured distortions. The output of the program is the bar configuration that minimizes SSD, which is defined in (3).

Two optimization commands are used to minimize SSD. SSD is minimized using a simplex solution method described by Nelder and Mead (1964) with the *fmins*( ) command (Grace 1990). SSD is also minimized using the *leastsq*( ) command, using a search algorithm based on Levenberg's (1944) and Marquardt's (1963) work. The algorithm used by *leastsq*( ), which is intended for least-squares problems, is described by More (1977).

One-Bar Problems

If it is assumed that only one steel bar is present, three variables need to be determined. These variables are the bar's horizontal location (x-coordinate), depth (y-coordinate), and area (A_{steel}). The initial trial values were $x = 0$, $y = 10$ mm, and $A_{steel} = 100$ mm^2. Assuming that only one bar is present makes it possible to simplify the algorithm. In particular, there is no distortion in the magnetic field at the bar due to magnetization of another bar. Therefore, $\mathbf{B}''$ in (1) is zero, and (2) may be ignored in step 5 of the algorithm.

The algorithm used to determine the location and size of one bar minimized SSD with both optimization commands. In almost all cases, both commands yielded the same results. In those few cases where the results differed, the result with the lowest SSD was selected as the algorithm's solution to the problem.

Two-Bar Problems

If two bars may be present, the number of variables doubles and the complexity of the governing equations increases. The number of unknown variables increases to six: two x-coordinate values, two y-coordinate values, and two area values. In addition, interaction between reinforcing bars must be considered because the magnetized steel in one bar will distort the magnetic field at the other bar [(2)].

The procedure used to identify as many as two bars involved solving the problem first as if one bar was present [Fig. 4(a)], and then as if two bars were present [Fig. 4(b)]. Initial trial values for the two-bar problems were $x = -10$ mm, $y = 10$ mm, and $A_{steel} = 100$ mm^2 for one bar and $x = 10$ mm, $y = 10$ mm, and $A_{steel} = 100$ mm^2 for the second bar. During preliminary investigations, the minimization commands often converged to a local minimum when two bars were close together. In particular, the computed configuration consisted

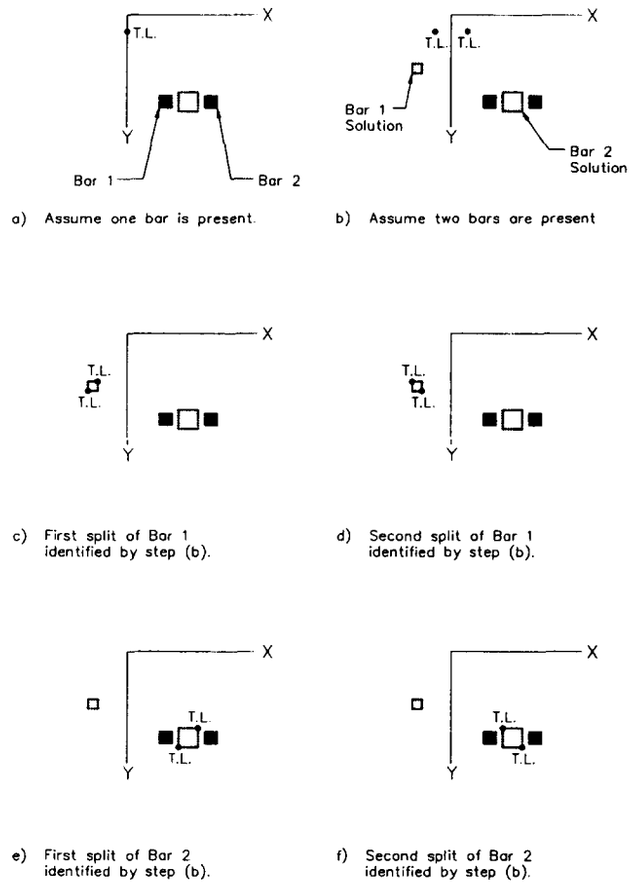

FIG. 4. Sequence of Initial Trial Locations (TL) for Two-Bar Search Algorithm

of one large bar at an intermediate position [Fig. 4(b)] and a second bar with an unrealistic location or an area that was either negative or excessively large.

To obtain the global minimum for SSD, four additional trial configurations were provided. The four additional configurations were based on the results of the first two-bar minimization. In particular, trial configurations for other two-bar solutions were selected that represented diagonal corners of one of the two bars identified by the initial two-bar solution. Both bars in the new trial configuration were assigned areas equal to one-half that of the bar being split. The splitting process was repeated so that both bars identified by the initial two-bar solution were split twice, once along each diagonal. The series of initial trial locations is described in Fig. 4. This process was performed with both optimization commands. The lowest SSD from the 12 solutions was selected as the best solution.

SIMULATIONS

Finite-element analyses were conducted on configurations containing rectangular steel bars to provide input data with which to test the reconstruction algorithm. All analyses were conducted with the same finite-element mesh. The model was prepared and analyzed with Ansoft Corp.'s Maxwell 2-D Field Simulator (*Maxwell* 1991), which uses a conjugate gradient method to solve magnetostatic problems. This finite-element model used 30,881 triangular elements to describe the geometry shown in Fig. 5. The outer boundary of the problem was located at a value of 200 mm in each coordinate direction. The conjugate gradient solver was allowed to perform 575 iterations on every problem simulated.

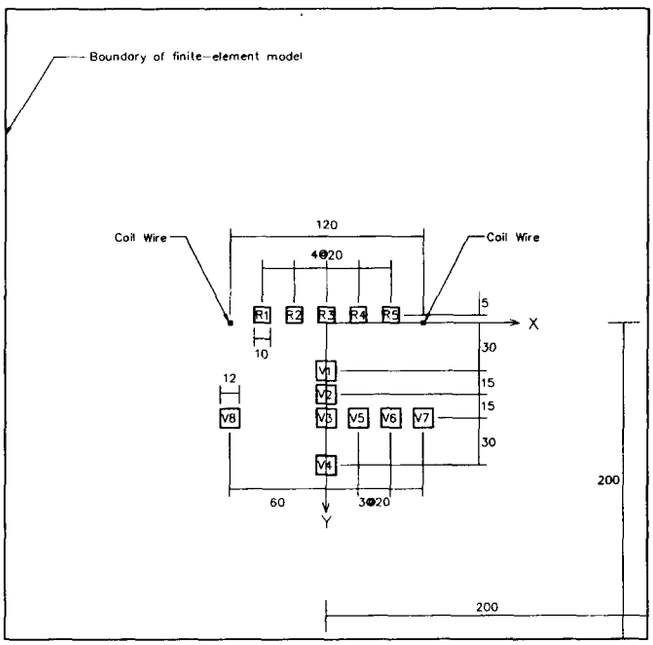

FIG. 5. Geometry of Finite-Element Model (All Units in Millimeters)

Two 2 by 2 mm wires with 1,000-A currents flowing in opposite directions were used to model the long coil. These wires were placed 120 mm apart center to center, symmetrically about the y-axis, and resting in the xz-plane. Five receiver locations were included in the model. They are denoted by R1–R5.

Eight possible locations for steel reinforcing bars were also provided. They are labeled V1–V8 in Fig. 5. Potential locations of reinforcing bars were 12 mm square in cross section, which corresponds to one-tenth of the coil's wire spacing. The cross-sectional area of 144 mm^2 was close to the nominal area of a No. 4 reinforcing bar, 127 mm^2. In locations where steel was present, the relative permeability was specified to be 2,000 (*CRC* 1992). In all other locations, the relative permeability was specified to be 1.0 (the value associated with free space).

To describe the bar geometries with nondimensional quantities, two parameters were defined. The ratio of bar depth to the distance between the coil wires was defined as the depth factor alpha, and the ratio of the x-coordinate to the distance between wires was defined as the horizontal location factor beta.

One-Bar Problems

Configurations containing one bar were analyzed with the bar located at x-coordinate equal to zero and increasing depths (y-coordinates) of 30, 45, 60, and 90 mm. These depths correspond to $\alpha = 0.25, 0.375, 0.5$, and 0.75. Configurations were also analyzed for a depth equal to one-half the coil wire spacing and x-coordinates of 0, 20, 40, and 60 mm. These x-coordinates correspond to β values of 0, 0.167, 0.333, and 0.5. Errors in the reconstructed coordinates were normalized with respect to the exact depth of the bar, and errors in reconstructed area were normalized with respect to the exact area.

Results for the one-bar problems are presented in Table 1. Normalized errors in the x- and y-coordinates were all less than 1.5%. They did not increase or decrease consistently with increasing coordinate values. The results also show that the error in bar area decreased as the x-coordinate or the y-coordinate of the bar increased. However, this decrease, less than 2.5% error over the range of α and β, was small compared with the total error in the bar areas (approximately 8–10%).

Two-Bar Problems

Configurations containing two bars were analyzed with the same finite-element mesh used to analyze the one-bar problems. Reconstructions were performed with the bars at various horizontal spacings and with the bars at various vertical spacings. In particular, effects of horizontal spacing were investigated by analyzing configurations 7-8, 3-7, 3-6, and 3-5, where the two numbers in each configuration name refer to the volume elements filled with steel (Fig. 5). The center-to-center bar spacing in each configuration was 120, 60, 40, and 20 mm, respectively. In all of these configurations the bar depths were 60 mm.

The results of implementing the two-bar search algorithm are reported in Table 2. Normalized errors from the exact values associated with these results are plotted against the ratio of bar depth to bar spacing for horizontally spaced bars in Fig. 6. Again, errors in the coordinates were normalized with respect to the exact depth of the bar, and errors in area were normalized with respect to the exact area. Fig. 6 shows that the algorithm effectively identified two horizontally spaced bars. The identification was successful even when the clear distance between the bars was less than the dimension of the bars (depth to spacing ratio of 2.5).

Effects of vertical spacing were investigated by analyzing configurations 1-4, 2-4, 3-4, and 2-3. Normalized errors from the algorithm's solutions for vertically spaced bars are plotted against the ratio of the depth of bar 2 (deepest bar) to the depth of bar 1 (shallowest bar) in Fig. 7. These plots show that the algorithm identified both bars with less than 20 percent error when the ratio of bar depths was 2 or less. The algorithm was unable to identify the bar farthest from the receivers when the ratio of bar depths was equal to 3. The closer bar masked the influence of the farther bar because the closer bar caused much greater distortion in the magnetic field. As the farthest bar's contribution to the distortion decreased in proportion to the contribution of the shallow bar, the problem became similar to a problem that contained only one bar.

SENSITIVITY TO MEASUREMENT ERROR

The error sensitivity of the proposed algorithm is an important consideration for future development because distortions in the magnetic field must be measured in the presence of a magnetic field of much greater intensity. For example, the ratios of $\mathbf{B}''$ to $\mathbf{B}_0$ ranged from about 0.0011 to 26 across the receivers when the bar was located at $\alpha = 0.25$ (depth of 30 mm) and $\beta = 0$. When α was increased to 0.75 (depth of 90 mm), the ratios ranged from 0.0006 to 0.9660. To quantify the algorithm's sensitivity to measurement errors, sensitivity analyses were performed for all one-bar configurations and for one two-bar configuration (configuration 7-8).

One-Bar Problems

For configurations containing one bar, each measured distortion was modified by the addition of induced random errors. The induced errors had a mean of zero and standard deviation σ calculated as follows:

$$\sigma = \xi \sqrt{\frac{(\mathbf{B}'')^T(\mathbf{B}'')}{n}} \tag{10}$$

where ξ ranged from 1–20%; and n = the number of components in $\mathbf{B}''$ (twice the number of receivers). At each percentage level of induced error, the reconstruction was per-

TABLE 1. Locations and Sizes Determined for One-Bar Problems[a]

Alpha: y_o/w[a] (1)	Beta x_o/w[a] (2)	Exact Values x_o (mm) (3)	Exact Values y_o (mm) (4)	Exact Values A_o (mm²) (5)	Minimization Results x (mm) (6)	Minimization Results y (mm) (7)	Minimization Results A (mm²) (8)	Normalized Error x (%) (9)	Normalized Error y (%) (10)	Normalized Error A (%) (11)
(*a*) Varying Horizontal Location										
0.5	0	0	60	144	0	60.0	156.0	0.0	0.0	8.3
0.5	0.167	20	60	144	19.5	59.9	155.5	0.8	0.2	8.0
0.5	0.333	40	60	144	39.1	59.7	154.9	1.5	0.5	7.6
0.5	0.5	60	60	144	59.5	59.4	154.0	0.8	1.0	6.9
(*b*) Varying Vertical Location										
0.25	0	0	30	144	0	30.3	158.5	0.0	1.0	10.1
0.375	0	0	45	144	0	45.1	156.8	0.0	0.2	8.9
0.5	0	0	60	144	0	60.0	156.0	0.0	0.0	8.3
0.75	0	0	90	144	0	89.9	155.1	0.0	0.1	7.7

[a]w is the width of the coil (120 mm).

TABLE 2. Locations and Sizes Determined for Two-Bar Problems

	BAR 1						BAR 2					
	Exact Values			Results			Exact Values			Results		
Bar configuration (1)	x (mm) (2)	y (mm) (3)	A_{steel} (mm²) (4)	x (mm) (5)	y (mm) (6)	A_{steel} (mm²) (7)	x (mm) (8)	y (mm) (9)	A_{steel} (mm²) (10)	x (mm) (11)	y (mm) (12)	A_{steel} (mm²) (13)
(*a*) Horizontally Spaced Bars												
7-8	−60	60	144	−59.4	59.2	152.5	60	60	144	59.4	59.0	151.1
3-7	0	60	144	−0.9	59.0	141.9	60	60	144	57.3	61.4	174.4
3-6	0	60	144	−2.2	58.2	122.5	40	60	144	36.2	61.6	192.6
3-5	0	60	144	−1.6	59.1	133.8	20	60	144	19.3	60.2	168.6
(*b*) Vertically Spaced Bars												
1-4	0	30	144	0	30.9	169.3	0	90	144	1.4	129.5	302.7
2-4	0	45	144	0	45.6	165.2	0	90	144	0.1	92.7	144.1
3-4	0	60	144	0	59.5	135.0	0	90	144	0	83.7	154.3
2-3	0	45	144	0	46.2	155.6	0	60	144	0	58.6	117.1

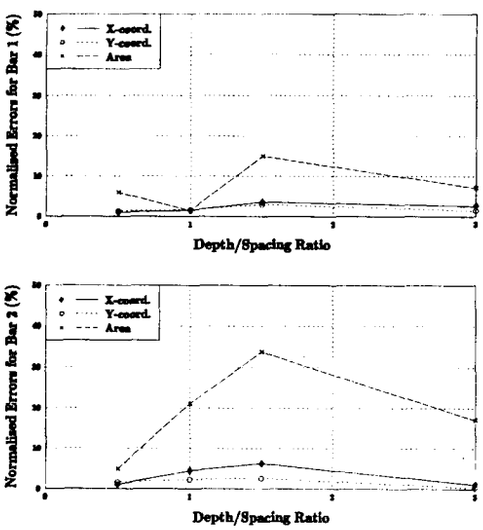

FIG. 6. Effects of Horizontal Spacing

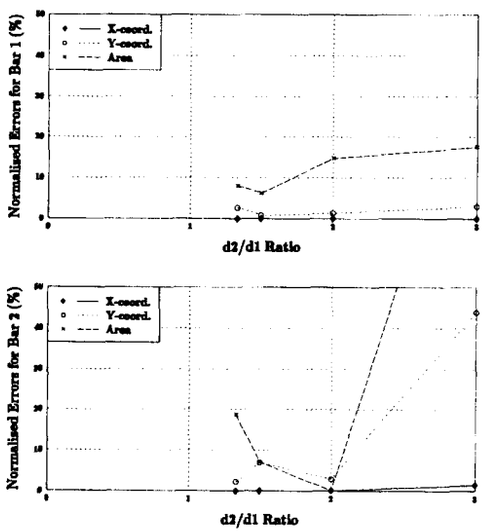

FIG. 7. Effects of Vertical Spacing

formed 50 times, each time with new random errors. The minimization routine used to solve problems containing one bar was then used to determine the location and size of each bar for each set of erroneous simulated measurements.

The mean absolute normalized errors from the algorithm solutions were plotted against the percentage of induced error. These plots are shown for a bar with varying depth in Fig. 8 and for a bar with varying x-coordinate in Fig. 9. These plots show that error sensitivity increased with increasing bar depth or x-coordinate value. Nevertheless, even when as much as 20% error was induced in the measured distortions, errors in resulting bar locations were less than 15%. Errors in determined bar areas were all less than 50%, which would result in an error of no more than one bar size for a No. 4 reinforcing bar.

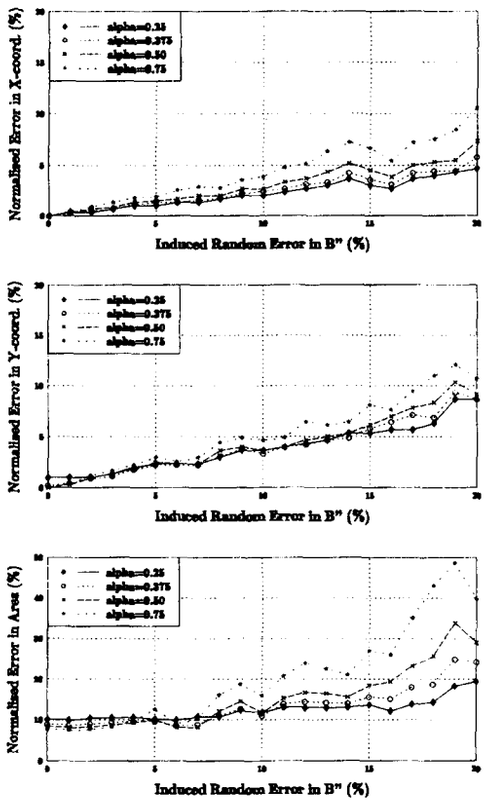

FIG. 8. Single Bar with Increasing Depth

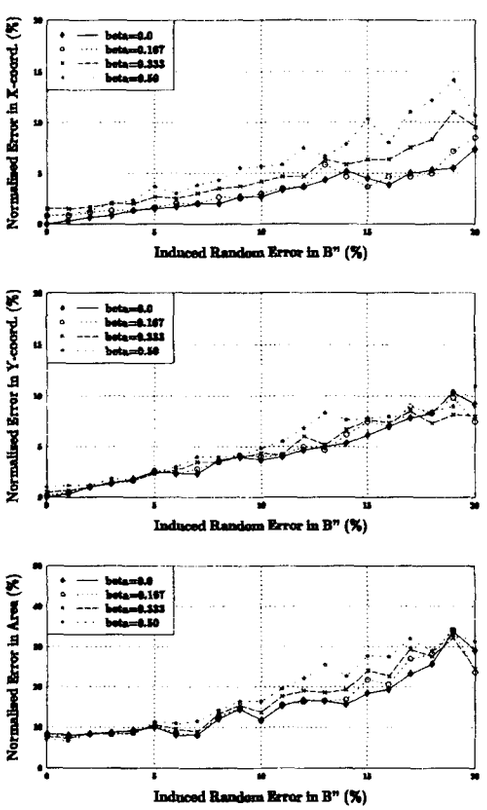

FIG. 9. Single Bar with Increasing x-Coordinate

Two-Bar Problems

A similar error analysis was conducted on bar configuration 7-8 (Fig. 5). In this error analysis, the induced errors ranged from 1%–10%. Solution errors in coordinates and areas, normalized as before, are plotted against the induced error in Fig. 10. These plots show that when the induced error in B″ exceeded 3%, the area values determined by the search algorithm differed greatly from the exact values.

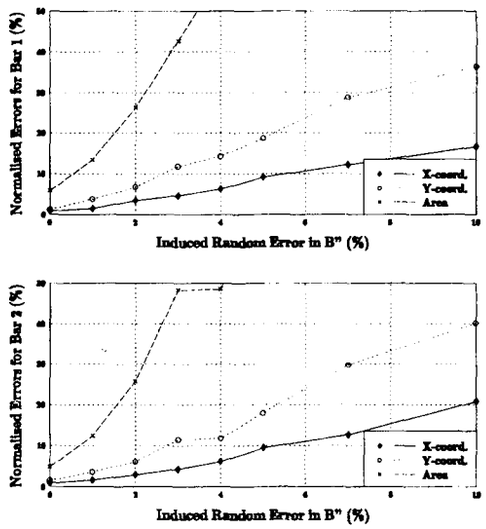

FIG. 10. Sensitivity Analysis for Configuration 7-8

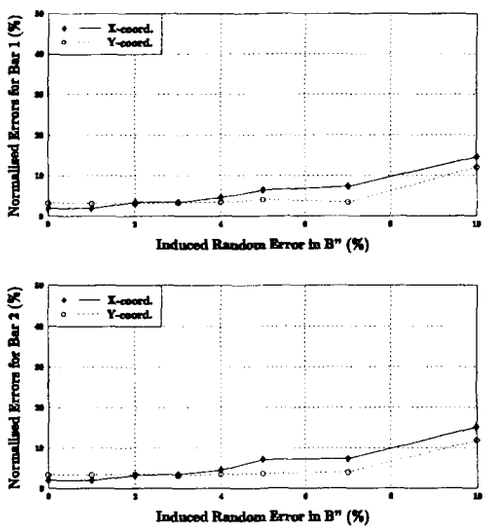

FIG. 11. Sensitivity Analysis with A_{steel} Set Equal to 144 mm² for Both Bars

The sensitivity analysis was repeated with A_{steel} for both bars held at 144 mm², representing a scenario in which the bar sizes are known and the locations need to be determined. Consequently, there were only four unknown variables in the problem (x- and y-coordinates for two bars). Plots of normalized errors in the x- and y-coordinates against induced error are provided in Fig. 11. The algorithm's sensitivity to errors decreased when the bar areas were known in advance. In fact, the largest normalized error was approximately 15% when 10% error was induced in the magnetic measurements. This error corresponds to 9 mm, which is less than the bar dimension.

These observations demonstrate that the algorithm required accurate measurements to determine the area of more than one bar. However, if the areas of the bars were already known, the algorithm identified the locations of the bars even in the presence of errors. Design and selection of measurement equipment should be based on the information provided by these sensitivity analyses.

COMPARISON WITH THREE-DIMENSIONAL ALGORITHM

The two-dimensional algorithm presented here is similar to the three-dimensional algorithm presented by Pla et al. (1994). Both rely on fundamental magnetostatic relationships that describe the interaction between steel reinforcement and an imposed magnetic field.

In the previous algorithm, the three-dimensional space was discretized into small volume elements, and the unknowns were the volumes of steel in the volume elements. The discretization approach is attractive because the steel in each volume element can be determined by solving a set of linear equations. No iteration is required. A disadvantage of the discretization approach is that it is necessary to measure the magnetic field at a number of locations at least equal to the number of volume elements. Many measurements would be required to obtain reasonable resolution in three dimensions.

An important advantage of the new algorithm is the great reduction in the number of measurements it requires. In the new formulation, only two components of **B** must be measured, and the number of unknowns is equal to three times the number of bars. The disadvantage of the new algorithm is the increase in computational effort. Whereas the previous formulation required that a set of linear equations be solved, the problem has been recast as an optimization problem. Nevertheless, the problem can be implemented on a personal computer.

Another consideration is the difference in error sensitivity between the algorithms. Errors in the finite-element simulation greatly affected the results of the three-dimensional reconstruction (Pla et al. 1994). The two-dimensional algorithm is much less sensitive to errors. The decreased sensitivity results from the fact that the distortion caused by a unit volume of steel is small compared with the distortion caused by a unit area of steel that extends to infinity in the third dimension.

CONCLUSIONS

In applications requiring the detection of a single reinforcing bar, the proposed imaging algorithm accurately determined the location and size of the bar. The algorithm's ability to identify a single bar did not appear to be sensitive to the errors induced by the researchers in the measurements of magnetic distortion.

It was also possible for the imaging algorithm to identify the locations of two bars if the bar depths were approximately the same. If one of the two bars was much closer to the receivers, only the closest bar was accurately identified by the algorithm. For problems involving two bars with unknown areas, the present formulation of the algorithm was unable to identify either bar accurately when small errors were induced in the measured distortions. If the areas of both bars were known, the algorithm was able to locate both bars accurately, even in the presence of 10% induced error.

ACKNOWLEDGMENTS

This research was funded by grant MSS-9158152 from the National Science Foundation. Sponsorship was also provided by the University of Washington Thomas and Marilyn Nielsen Endowed Fund in Engineering.

APPENDIX. REFERENCES

Bleaney, B. I., and Bleaney, B. (1965). *Electricity and magnetism*. Oxford University Press, London, England.

CRC handbook of chemistry and physics. (1992). 73rd Ed., CRC Press, Boca Raton, Fla.

Grace, A. (1990). *Optimization Toolbox: For use with MATLAB*. The MathWorks, Inc., Natick, Mass.

Lauer, K. R. (1991). "Magnetic electrical methods." *Handbook on nondestructive testing of concrete*, V. M. Malhotra, and N. J. Carino, eds., CRC Press, Boca Raton, Fla., 203–225.

Levenberg, K. (1944). "A method for the solution of certain problems in least squares." *Quart. Appl. Math.*, 2(2), 164–168.

Marquardt, D. (1963). "An algorithm for least-squares estimation of nonlinear parameters." *SIAM J. Appl. Math.*, 11, 431–441.

Maxwell 2D Field Simulator Users Guide. (1991). Ansoft Corp., Pittsburgh, Pa.

More, J. J. (1977). "The Levenberg-Marquardt algorithm: Implementation and theory." *Numerical Analysis, Lecture Notes in Mathematics 630*, Watson, G. A., ed., Springer-Verlag, Berlin, West Germany, 105–116.

Nayfeh, M. H., and Brussel, M. K. (1985). *Electricity and magnetism*. John Wiley, New York, N.Y.

Nelder, J. A., and Mead R. (1964). "A simplex method for function minimization." *Comput. J.*, 7(4), 308–313.

Pla, G., Eberhard, M., and Eberhard, P. (1994). "Magnetic imaging of reinforcing steel." *J. Nondestructive Evaluation*, 13(1), 23–32.

Sigmon, K. (1992). *MATLAB Primer*. 2nd ed., Dept. of Math., Univ. of Florida, Gainesville, Fla.